JNPS 10 (2): 145 – 151 (2024)
ISSN: 2392-473X (Print), 2738-9537 (Online)

Research Article ©*Nepal Physical Society*
doi.org/10.3126/jnphyssoc.v10i2.79466

Relativistic Tight-Binding Model for Hexagonal Lattice: Application to Graphene

Rohin Sharma,[1] Dipendra Bahadur Hamal,[1,*)] Kaustav Regmi,[1] Amit Shrestha,[2,†)] Katsuhiko Higuchi,[2] and Masahiko Higuchi[3]

[1)]*Department of Physics, Kathmandu University, Dhulikhel, Nepal*
[2)]*Graduate School of Advanced Science of Matter, Hiroshima University, Higashi-Hiroshima 739-8527, Japan*
[3)]*Department of Physics, Faculty of Science, Shinshu University, Matsumoto, Nagano 390-8621, Japan*

Abstract. A non-perturbative relativistic tight-binding (TB) approximation method applicable to crystalline material immersed in a magnetic field was developed and tested for crystalline silicon in 2015. To apply this method to any material in a magnetic field, the electronic structure of the material in absence of the magnetic field must be calculated. In this study, we present the relativistic TB approximation method for graphene in a zero magnetic field. The Hamiltonian and overlap matrices are constructed considering the nearest neighboring atomic interactions between the *s* and *p* valence orbitals, where the relativistic hopping and overlap integrals are calculated using the relativistic version of the Slater-Koster table. The method of constructing the Hamiltonian and overlap matrices and the resulting energy-band structure of graphene in the first Brillouin zone is presented in this paper. The appearance of a small band-gap at the *k*-points (also known as the spin-orbit gap) due to the relativistic effect seen at low temperature whose magnitude is 25 μeV, have also been shown by the theory.

Submitted: August 11, 2024; **Revised**: May 30, 20254; **Accepted**:June 1, 2025

Keywords: MFRTB approximation method; TB method; Relativistic TB parameter; spin orbit coupling; crystal field energy

Introduction

The popularity of graphene research mainly stems from its unique and fascinating electronic [1, 2] and magnetic properties [3, 4] and also due to the promise of potential applications [5, 6] and the emergence of a new paradigm of relativistic-condensed matter physics [7]. Some of these physical properties are: its minimum conductance never falls below the value corresponding to the smallest quantum unit of conductance even when the charge carrier concentrations tend to zero [1], tunable conductivity in twisted monolayer-bilayer graphene system, insulating behavior at low temperatures [2], half-integer quantum Hall effect [4], unconventional magnetic oscillations [8] and strong orbital diamagnetism [9]. The anomalous electronic properties of graphene arise from its characteristic band structure which is due to the effectively massless charge carriers with relativistic behavior known as Dirac fermions at energies near the Fermi level where the conical valence band and conduction band meet at a single point in momentum space called the Dirac points.

Because of these physical properties of graphene, it is desirable to investigate a first principle calculation method that takes into account both the relativistic effect and magnetic field. There are several studies where the electronic structure is calculated with a non-relativistic tight-binding model [10, 11] and a large number of these studies have been without considering the overlap integral [3, 11, 12]. There also exists a lot of credible relativistic calculation methods of electronic structures in the absence of a magnetic field [13–15] that have been successfully applied to f-electrons of rare earth compound $YbGa_2$ [15] and compound $CeRu_2$ [16], but the electronic structure calculation method that can deal with magnetic field and relativistic effects simultaneously is desired for the study.

In 2015 a Non-perturbative Tight-Binding (TB) method called the magnetic-field-containing relativistic tight-binding approximation method (MFRTB method) was developed incorporating both the relativistic effects and magnetic field in the same footing and was applied to sili-

*)Corresponding author: dipendra.hamal@ku.edu.np
†)Corresponding author: shrestha.amit.908@m.kyushu-u.ac.jp

con crystal immersed in magnetic field [17]. The MFRTB method was developed to alternatively describe the oscillatory behavior of the magnetization as a function of the magnetic field (the de Haas-van Alphen effect) from a viewpoint of the first-principle calculation. The MFRTB method was successfully able to calculate the relativistic energy band structures of silicon in an external magnetic field [17] that explained the suppression of softening in the elastic constant of boron-doped silicon in an external magnetic field and also revisited the dHvA effect in a first-principle way [18]. This method also presents the relativistic version of the Slater-Koster table in which the relativistic hopping integrals are explicitly expressed in terms of relativistic TB parameters for the interactions corresponding to $2s$ and $2p$ orbitals.

In order to apply the MFRTB method to materials in magnetic fields, the magnetic hopping integrals must be expressed in terms of the relativistic hopping integrals for zero magnetic fields and a magnetic field-dependent phase factor. So as an initial step, we need to formulate a relativistic TB model in zero magnetic field. A key novelty of this work is the application of the relativistic TB model to hexagonal lattices in the absence of magnetic fields, providing a foundation for future studies involving magnetic fields. This has significant implications for understanding relativistic effects in 2D materials and crystalline systems. Hence, a relativistic TB model for graphene in the absence of a magnetic field is formulated, starting from the Dirac equation for an electron in a periodic potential. The Dirac Hamiltonian matrix and overlap matrix of the system are then constructed utilizing the relativistic Slater-Koster table considering the nearest neighbor interactions between $2s$ and $2p$ orbitals. By solving the general eigenvalue equation for different k-points in the first Brillouin zone, the relativistic electronic structure of graphene is obtained.

Hence, in this study we tried to address a critical area in condensed matter physics, specifically the use of relativistic effects of the tight-binding (TB) model on hexagonal lattices. Our results have shown the appearance of a band gap of 25 μeV for graphene at the Dirac points due to the spin-orbit coupling (SOC), which is in excellent agreement with the first principle calculation results of graphene using the linearized augmented plane-wave method incorporating the SOC [19].

Relativistic TB theory for graphene lattice in zero magnetic field

Considering the two atoms of the unit cells of the honeycomb lattice, we proceed to establish the equations for the Hamiltonian matrix elements and the overlap matrix elements of the system. We represent the two atoms of the unit cell as 'A' and 'B', as shown in Figure 1.

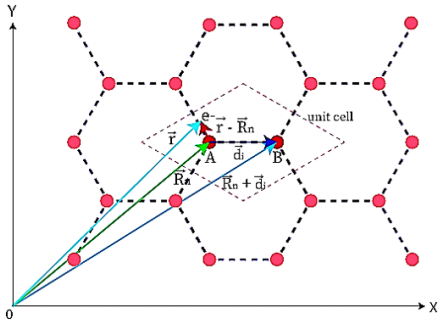

FIGURE 1: Illustration of a honeycomb lattice and unit cell of graphene.

For lattice site 'A'

The Dirac equation for an electron at lattice site 'A' is

$$\hat{H}_A \Psi_{\alpha,\vec{k}}(\vec{r}) = E(\vec{k}) \Psi_{\alpha,\vec{k}}(\vec{r}) \tag{1}$$

with the atomic Hamiltonian at site 'A' as

$$\hat{H}_A = c\vec{\alpha} \cdot \vec{p} + \beta mc^2 + V_A(\vec{r} - \vec{R}_n) \tag{2}$$

Where c denotes the velocity of light, m denotes the electron rest mass, $\vec{\alpha} = (\alpha_x, \alpha_y, \alpha_z), \beta$ stands for the usual 4×4 matrices [20], $V_A(\vec{r} - \vec{R}_n)$ represents the Coulomb potential due to the nucleus of the atom at site 'A' located at $\vec{R}_n$, the subscripts α and $\vec{k}$ of the eigenfunction $\Psi_{\alpha,\vec{k}}(\vec{r})$ represents the band index and crystal momentum respectively.

Expanding$\Psi_{\alpha,\vec{k}}(\vec{r})$ by using the Bloch sum of relativistic atomic orbital $\phi^A_{nlJM}(\vec{r})$ of atom at 'A' as the basis function, we have

$$\Psi_{\alpha,\vec{k}}(\vec{r}) = \sum_{nlJM} C^A_{nlJM,\vec{K}} B^A_{nlJM}(\vec{r}) \tag{3}$$

where $C^A_{nlJM,\vec{K}}$ is the expansion coefficient and $B^{A,\vec{k}}_{nlJM}(\vec{r})$ denote the Bloch sum which is written as

$$B^{A,\vec{k}}_{nlJM}(\vec{r}) = \frac{1}{\sqrt{N}} \sum_{\vec{R}_n} e^{i\vec{k}\cdot\vec{R}_n} \phi^A_{nlJM}\left(\vec{r} - \overrightarrow{R_n}\right). \tag{4}$$

The n,l,M, and J in Eq. (4) are the principle, angular momentum, total angular momentum, and magnetic quantum numbers respectively. Here the relativistic atomic orbital obeys the following Dirac equation;

$$\begin{aligned}\left[c\vec{\alpha} \cdot \vec{p} + \beta mc^2 + V_A\left(\vec{r} - \vec{R}_n\right)\right] \phi^A_{nlJM}\left(\vec{r} - \overrightarrow{R_n}\right) \\ = \varepsilon^A_{nlJ} \phi^A_{nlJM}\left(\vec{r} - \overrightarrow{R_n}\right)\end{aligned} \tag{5}$$

where ε^A_{nlJ} denotes the atomic spectrum for zero magnetic field at site 'A', which is independent of M. Multiplying by $\phi^{\dagger A'}_{n'l'J'M'}(\vec{r} - \vec{R}_{n'})$ where $\vec{R}_{n'} \neq \vec{R}_n$, $A' \neq A$ and integrating and denoting the hopping and overlap integrals by

$t^{A'A}_{n'l'J'M',nlJM}(\vec{R}_n-\vec{R}_{n'})$ and $s^{A'A}_{n'l'J'M',nlJM}(\vec{R}_n-\vec{R}_{n'})$, respectively, the Hamiltonian and overlap matrix elements are defined as

$$\mathbf{H}^{A'}_{n'l'J'M',nlJM}(\vec{k})=\sum_{\vec{R}_n}e^{i\vec{k}\cdot\overrightarrow{R_n}}t^{A'A}_{n'l'J'M',nlJM}\left(\overrightarrow{R_n}-\overrightarrow{R_{n'}}\right) \quad (6)$$

and

$$\mathbf{S}^{A'}_{n'l'J'M',nlJM}(\vec{k})=\sum_{\overrightarrow{R_n}}e^{i\vec{k}\cdot\overrightarrow{R_n}}S^{A'A}_{n'l'J'M',nlJM}\left(\overrightarrow{R_n}-\vec{R}_{n'}\right). \quad (7)$$

So, Eq. (1) becomes

$$\sum_{nlJM}\mathbf{H}^{A'A}_{n'l'J'M',nlJM}(\vec{k})C^{A}_{nlJM,\vec{K}} = E(\vec{k})\sum_{nlJM}\mathbf{S}^{A'A}_{n'l'J'M',nlJM}(\vec{k})C^{A}_{nlJM,\vec{k}} \quad (8)$$

After evaluating the relativistic hopping and overlap integrals when the lattice site is considered to be at the origin $\vec{R}_n=0$, $d_i=d_j$ and when the lattice site is considered to be elsewhere $\vec{R}_n\neq 0$, $d_i\neq d_j$ and by neglecting the three center integral, we get the matrix elements of the Hamiltonian and overlap Eq. (6) and Eq. (7) as:

$$\mathbf{H}^{A'A}_{n'l'J'M',nlJM}(\vec{k}) = \left(\varepsilon^{A}_{nlJ}+\Delta\varepsilon^{A}_{nlJM}\right)\delta_{n'l'J'M',nlJM}\delta_{i,j} + \sum_{\vec{R}_n}e^{i\vec{k}\cdot\vec{R}_n}\left(1-\delta_{\vec{R}_n,0}\delta_{i,j}\right)t^{new,A'A}_{n'l'j'M',nlJM}\left(\vec{R}_n\right), \quad (9)$$

with

$$t^{new,A'A}_{n'l'J'M',nlJM}(\vec{R}_n) = \frac{1}{2}\left(\varepsilon^{A}_{nlJ}+\varepsilon^{A'}_{n'l'J'}\right)s^{A'A}_{n'l'J'M',nlJM}(\vec{r}-\vec{R}_n) + \int\phi^{\dagger A'}_{n'l'J'M'}(\vec{r})\left(\frac{V_{A'}(\vec{r})+V_A(\vec{r}-\vec{R}_n)}{2}\right)\phi^{A}_{nlJM}(\vec{r}-\vec{R}_n)\,d^3\vec{r} \quad (10)$$

where $\Delta\varepsilon^{A}_{nlJM}$ is the crystal field energy due to the influence of other lattice sites on site 'A' written as

$$\Delta\varepsilon^{A}_{nlJM}=\int\phi^{\dagger A'}_{n'l'J'M'}(\vec{r}) \times\sum_{\vec{R}_m\neq\vec{R}_n}\sum_{A'\neq A}V_A(\vec{r}-\vec{R}_m)\,\phi^{A}_{nlJM}(\vec{r}-\vec{R}_m)\,d^3\vec{r}, \quad (11)$$

and

$$S^{A'A}_{n'l'J'M',nlJM}(\vec{k})=\delta_{n'l'J'M',nlJM}\,\delta_{i,j} +\sum_{\vec{R}_n}e^{i\vec{k}\cdot\vec{R}_n}\left(1-\delta_{\vec{R}_n,0}\,\delta_{i,j}\right)\times s^{A'A}_{n'l'J'M',nlJM}(\vec{R}_n), \quad (12)$$

with

$$s^{A'A}_{n'l'J'M',nlJM}(\vec{R}_n)=\int\phi^{\dagger A'}_{n'l'J'M'}(\vec{r})\,\phi^{A}_{nlJM}(\vec{r}-\vec{R}_n)\,d^3\vec{r} \quad (13)$$

For Lattice Site 'B'

Similarly, for the lattice site B located at $\vec{R}_n+\vec{d}_i$, where $\vec{d}_i$ is the position vector from site A to site B, we can formulate the Hamiltonian and overlap matrix elements as:

$$\mathbf{H}^{B'B}_{n'l'J'M',nlJM}(\vec{k}) = \left(\varepsilon^{B}_{nlJ}+\Delta\varepsilon^{B}_{nlJM}\right)\delta_{n'l'J'M',nlJM}\delta_{i,j} +\sum_{\vec{R}_n}e^{i\vec{k}\cdot\vec{R}_n}\left(1-\delta_{\vec{R}_n,0}\delta_{i,j}\right) \times t^{new,B'B}_{n'l'j'M',nlJM}\left(\vec{R}_n-\vec{d}_i+\vec{d}_j\right), \quad (14)$$

with

$$t^{new,B'B}_{n'l'J'M',nlJM}\left(\vec{R}_n-\vec{d}_i+\vec{d}_j\right) = \frac{1}{2}\left(\varepsilon^{B}_{nlJ}+\varepsilon^{B'}_{n'l'J'}\right)s^{B'B}_{n'l'J'M',nlJM}\left(\vec{r}-\vec{R}_n-\vec{d}_i+\vec{d}_j\right) + \int\phi^{\dagger B'}_{n'l'J'M'}(\vec{r})\left(\frac{V_{B'}(\vec{r})+V_B(\vec{r}-\vec{R}_n)}{2}\right) \times\phi^{B}_{nlJM}\left(\vec{r}-\vec{R}_n-\vec{d}_i+\vec{d}_j\right)d^3\vec{r} \quad (15)$$

where $\Delta\varepsilon^{B}_{nlJM}$ is the crystal field energy due to the influence of other lattice sites on site 'B' written as

$$\Delta\varepsilon^{B}_{nlJM}=\int\phi^{\dagger B'}_{n'l'J'M'}(\vec{r}) \times\sum_{\vec{R}_m\neq\vec{R}_n}\sum_{B'\neq B}V_B\left(\vec{r}-\vec{R}_n-\vec{d}_i+\vec{d}_j\right) \times\phi^{B}_{nlJM}\left(\vec{r}-\vec{R}_n-\vec{d}_i+\vec{d}_j\right)d^3\vec{r}, \quad (16)$$

and

$$S^{B'B}_{n'l'J'M',nlJM}\left(\vec{r}-\vec{R}_n-\vec{d}_i+\vec{d}_j\right) = \delta_{n'l'J'M',nlJM}\,\delta_{i,j} +\sum_{\vec{R}_n}e^{i\vec{k}\cdot\vec{R}_n}\left(1-\delta_{\vec{R}_n,0}\,\delta_{i,j}\right) \times s^{B'B}_{n'l'J'M',nlJM}\left(\vec{R}_n-\vec{d}_i+\vec{d}_j\right), \quad (17)$$

with

$$s^{B'B}_{n'l'J'M',nlJM}\left(\vec{R}_n-\vec{d}_i+\vec{d}_j\right) =\int\phi^{\dagger B'}_{n'l'J'M'}(\vec{r})\,\phi^{B}_{nlJM}\left(\vec{R}_n-\vec{d}_i+\vec{d}_j\right)d^3\vec{r}. \quad (18)$$

Hamiltonian and Overlap Matrix Elements of the System

The equations of Hamiltonian matrix elements for sites 'A' and 'B' differ only in the position of lattice sites, so formulating a general form of the Hamiltonian and overlap matrix elements considering the nearest neighboring interactions in a hexagonal lattice,

$$\hat{H}_{n'l'J'M',nlJM}(\vec{k}) = (\varepsilon_{nlJ} + \Delta\varepsilon_{nlJM})\,\delta_{n'l'J'M',nlJM}\delta_{ij} + \left(1 - \delta_{\vec{R}_n,0}\delta_{ij}\right)\sum_{\vec{R}_n}\sum_{i=1}^{3} e^{i\vec{k}\cdot(\vec{R}_n+\vec{d}_i)} \times t^{\text{new}}_{n'l'J'M',nlJM}(\vec{R}_n - \vec{d}_i + \vec{d}_j) \tag{19}$$

and

$$\hat{S}_{n'l'J'M',nlJM}(\vec{k}) = (\varepsilon_{nlJ} + \Delta\varepsilon_{nlJM})\,\delta_{n'l'J'M',nlJM}\delta_{ij} + \left(1 - \delta_{\vec{R}_n,0}\delta_{ij}\right)\sum_{\vec{R}_n}\sum_{i=1}^{3} e^{i\vec{k}\cdot(\vec{R}_n+\vec{d}_i)} \times s^{\text{new}}_{n'l'J'M',nlJM}(\vec{R}_n - \vec{d}_i + \vec{d}_j) \tag{20}$$

Here $i = 1,2,3$; as only the first nearest neighbors atoms of the site A or B was considered in a honeycomb lattice of graphene with d_i as their position vectors. The superscripts 'A' and 'B' are eliminated because both are carbon atoms. Then Eq. (8) is rewritten as:

$$\sum_{nlJM}\Bigg[(\varepsilon_{nlJ} + \Delta\varepsilon_{nlJM})\,\delta_{n'l'J'M',nlJM} + \sum_{\vec{R}_n}\sum_{i=1}^{3} e^{i\vec{k}\cdot(\vec{R}_n+\vec{d}_i)}\left(1 - \delta_{\vec{R}_n,0}\delta_{ij}\right) \times t^{\text{new}}_{n'l'J'M',nlJM}(\vec{R}_n - \vec{d}_i + \vec{d}_j)\Bigg] C^{i}_{nlJM,\vec{k}}$$
$$= E(\vec{k})\Bigg[\delta_{n'l'J'M',nlJM}\delta_{ij} + \sum_{\vec{R}_n}\sum_{i=1}^{3} e^{i\vec{k}\cdot(\vec{R}_n+\vec{d}_i)}\left(1 - \delta_{\vec{R}_n,0}\delta_{ij}\right) \times s^{new}_{n'l'J'M',nlJM}(\vec{R}_n - \vec{d}_i + \vec{d}_j)\Bigg] C^{i}_{nlJM,\vec{k}} \tag{21}$$

Eq. (21) is the simultaneous equation which is to be solved to obtain the energy eigenvalues $E(\vec{k})$.

Method

Construction of Hamiltonian and Overlap Matrix of the system

For our calculations, we have considered the atomic states of $2s$ and $2p$ valance orbitals of carbon atom so the interactions are among the following 8 atomic states: (2,0,1/2,1/2),(2,0,1/2,-1/2),(2,1,1/2,1/2),(2,1,3/2,1/2), (2,1,1/2,-1/2), (2,1,3/2,-1/2), (2,1,3/2,3/2) and (2,1,3/2,-3/2). For these atomic interactions, we constructed the Hamiltonian and overlap matrix using Eq. (19) and Eq. (20). To obtain the numerical values of $t^{\text{new}}_{n'l'J'M',nlJM}(\vec{R}_n - \vec{d}_i + \vec{d}_j)$ and $s^{\text{new}}_{n'l'J'M',nlJM}(\vec{R}_n - \vec{d}_i + \vec{d}_j)$ we used the relativistic version of the Slater-Koster table [17] to express the hopping and overlap integrals in terms of the TB parameters $K_d^{(i,j)}(n'l'J',nlJ)_{|M|}$ and $S_d^{(i,j)}(n'l'J',nlJ)_{|M|}$ and then solved Eq. (10) and Eq. (12). Since the crystal field energy is very small compared to the atomic spectrum, we have neglected $\Delta\varepsilon_{nlJM}$ and used the atomic spectrum ε_{nlJM} that is calculated using density functional theory [21, 22] based on local density approximation [23]. The numerical values of the term $\varepsilon_{nlJ} + \Delta\varepsilon_{nlJM}$ are listed in Table I. The numerical values of the TB parameters for the 8 atomic states of the nearest neighboring atoms of graphene $K_d^{(i,j)}(n'l'J',nlJ)_{|M|}$ and $S_d^{(i,j)}(n'l'J',nlJ)_{|M|}$ has been calculated [23] which are listed in Table II.

Energy States	Numerical Values (eV)
$\varepsilon_{20\ 1/2} + \Delta\varepsilon_{20\ 1/2\ M}$	-8.37
$\varepsilon_{21\ 1/2} + \Delta\varepsilon_{21\ 1/2\ M}$	0
$\varepsilon_{21\ 3/2} + \Delta\varepsilon_{21\ 3/2\ M}$	8.305×10^{-3}

TABLE I: Numerical values of the sum of electronic spectra and crystal field energy [23].

To solve Eq. (21) we first constructed a 16×16 Hamiltonian and overlap matrices using the values from Table (1) and Table (2) and using Eq. (19) and Eq. (20) for the 8 atomic states at sites A, B and A', B'. The first term vanishes for the non-diagonal elements (since $n'l'J'M' \neq nlJM$ and $i \neq j$) and the second term vanishes for the diagonal elements (since $i = j$ and $\vec{R}_n = 0$).

Electronic Structure Calculation

Considering an atom to be at the origin, the coordinates of its three nearest neighbors are $\left(\frac{a}{\sqrt{3}}, 0\right)$, $\left(-\frac{a}{\sqrt{3}}, \frac{a}{2}\right)$,

$(nlJM)$	**Numerical Values (eV)**
$K_1(20\ \frac{1}{2},\ 20\ \frac{1}{2})_{\frac{1}{2}}$	-5.727
$K_1(20\ \frac{1}{2},\ 21\ \frac{1}{2})_{\frac{1}{2}}$	-3.226
$K_1(20\ \frac{1}{2},\ 21\ \frac{3}{2})_{\frac{1}{2}}$	4.587
$K_1(21\ \frac{1}{2},\ 21\ \frac{1}{2})_{\frac{1}{2}}$	-1.81×10^{-2}
$K_1(21\ \frac{1}{2},\ 21\ \frac{3}{2})_{\frac{1}{2}}$	-4.298
$K_1(21\ \frac{3}{2},\ 21\ \frac{3}{2})_{\frac{1}{2}}$	3.01
$K_1(21\ \frac{3}{2},\ 21\ \frac{3}{2})_{\frac{3}{2}}$	-3.064
$S_1(20\ \frac{1}{2},\ 20\ \frac{1}{2})_{\frac{1}{2}}$	1.012×10^{-1}
$S_1(20\ \frac{1}{2},\ 21\ \frac{1}{2})_{\frac{1}{2}}$	9.739×10^{-2}
$S_1(20\ \frac{1}{2},\ 21\ \frac{3}{2})_{\frac{1}{2}}$	-1.392×10^{-1}
$S_1(21\ \frac{1}{2},\ 21\ \frac{1}{2})_{\frac{1}{2}}$	-7.904×10^{-2}
$S_1(21\ \frac{1}{2},\ 21\ \frac{3}{2})_{\frac{1}{2}}$	2.081×10^{-1}
$S_1(21\ \frac{3}{2},\ 21\ \frac{3}{2})_{\frac{1}{2}}$	-2.289×10^{-1}
$S_1(21\ \frac{3}{2},\ 21\ \frac{3}{2})_{\frac{3}{2}}$	6.802×10^{-2}

TABLE II: Relativistic TB parameters for the hopping and overlap integrals for nearest neighboring graphene atoms.

and $\left(-\frac{a}{\sqrt{3}}, -\frac{a}{2}\right)$ where $a = 2.4$ Å is the lattice constant. It can be shown that the position coordinates of the high symmetry points in the reciprocal lattice, as shown in Figure 2, are as follows:

$$\begin{aligned} \Gamma &= (0,\ 0) \\ K &= \left(\frac{2\pi}{a\sqrt{3}}, \frac{2\pi}{3a}\right) \\ M &= \left(\frac{2\pi}{a\sqrt{3}},\ 0\right) \end{aligned} \tag{22}$$

After constructing the Hamiltonian and overlap matrix, we solved the general eigenvalue Eq. (8) along a closed contour $K-\Gamma-M-K$ in the $\vec{k}$ space to get the energy eigenvalues $E(\vec{k})$ and obtained the electronic band structure.

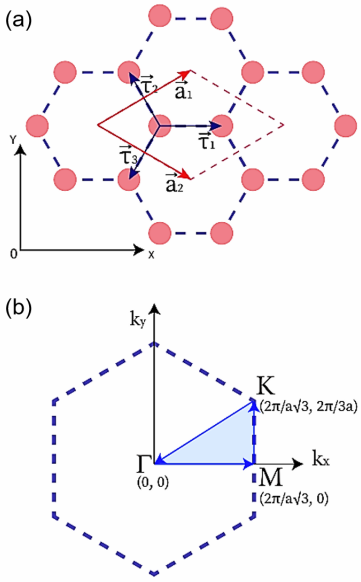

FIGURE 2: (a) Illustration of real lattice and unit cell of graphene. (b) Illustration of reciprocal lattice and first Brillouin zone of graphene.

Result and Discussion

The energy diagram obtained from the calculation along the closed contour $K-\Gamma-M-K$ is shown in Fig. (4). The obtained band gap energy at the K-point was 2.58×10^{-5} eV whose value is in close agreement with the value shown by the first-principle calculations considering spin-orbit interaction done by the FLAPW method [19]. Our approach remains valid and applicable for graphene because the spin-orbit gap value (≈ 25 μeV) obtained is in excellent agreement with first-principles calculations, confirming the adequacy of our relativistic SK parameterization. The absence of significant crystal field splitting in 2D honeycomb structures justifies its exclusion in our tight-binding framework. This method provides a computationally efficient yet accurate way to study relativistic effects in 2D materials, making it a practical tool for future investigations involving external fields or strain effects.

In graphene, the SOC-induced band gap is too small for practical observation, but its presence theoretically classifies graphene as a quantum spin Hall insulator in an idealized scenario. Experimentally, modifications via heavy adatom doping could enhance SOC and enable its spintronic applications [24].

Through this work, we have validated the success of a novel semi-empirical method relativistic TB method to calculate the electronic band structure of graphene considering relativistic effects. The success of the method is demonstrated by correctly predicting the splitting of

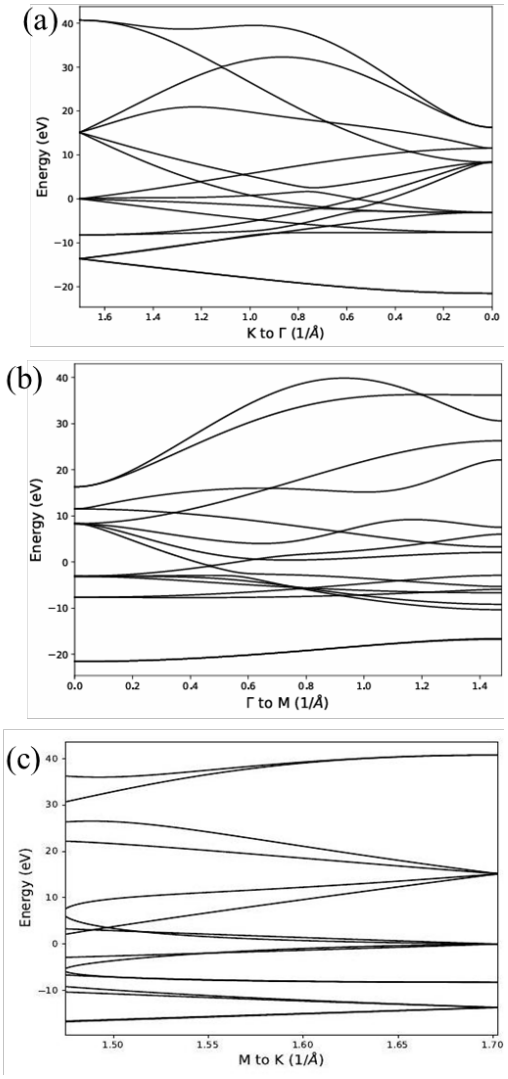

FIGURE 3: Band structure along the high symmetry points. (a) Energy bands from K to Γ (b) Energy bands from Γ to M. (c) Energy bands from M to K.

bands at the Dirac K-point. The magnetic field effects can also be incorporated into the present model by utilizing the magnetic Bloch theorem and approximating the magnetic hopping integrals as the relativistic hopping integrals multiplied by the magnetic field-dependent phase factor. In conclusion, this is a coherent relativistic tight-binding model that can be applied to accurately predict the relativistic effects for various systems.

Conclusion

In this study, we developed a relativistic tight-binding (TB) model for hexagonal lattices, starting from the Dirac equation and incorporating relativistic effects through the Slater-Koster approach. By constructing the Hamiltonian and overlap matrices and solving the eigenvalue equation, we obtained the electronic structure of graphene, demonstrating the impact of SOC. The result showed a band gap of $\approx 25\ \mu eV$, which aligns well with previous first-principles calculations, confirming the validity of our approach.

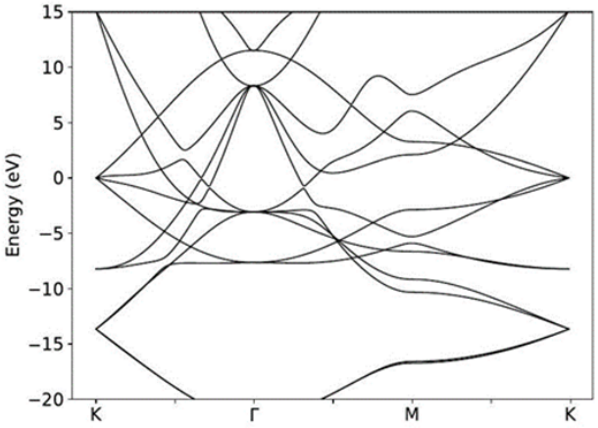

FIGURE 4: Enlarged view of the energy bands. The distinct $\pi\pi^*$ and σ bonding are successfully replicated.

Our method, based on the Dirac equation and Slater-Koster approach, offers a systematic and computationally efficient way to study the electronic structure of hexagonal lattices while incorporating relativistic effects. Since it only requires nearest-neighbor interactions and relativistic parameters, it can be easily extended to other 2D materials. Moreover, compared to first-principles methods, this TB framework provides an analytical understanding of SOC effects while significantly reducing computational cost. Its simplicity makes it a powerful tool for large-scale simulations and for exploring external field effects in condensed matter systems. These reflect the generality and ease of application of our method for future studies. Incorporation of magnetic field effect will be the focus of future work.

Corresponding Authors

Dipendra Bahadur Hamal–Department of Physics, Kathmandu University, Dhulikhel, Nepal.

Amit Shrestha–Center for Polymer Interface and Molecular Adhesion Science, Kyushu University 744 Motooka, Nishi–ku, Fukuoka 819–0395, Japan. (Current Address) Graduate School of Advanced Science of Matter, Hiroshima University, Higashi-Hiroshima 739-8527, Japan. (Previous Address)

Conflict of Interest

The authors declare no conflict interest.

Acknowledgment

This work was supported by the Department of Physics, Kathmandu University, Dhulikhel, Nepal.

REFERENCES

1. K. S. Novoselov, A. K. Geim, S. V. Morozov, D. Jiang, M. I. Katsnelson, I. Grigorieva, S. Dubonos, and A. A. Firsov, "Two-dimensional gas of massless dirac fermions in graphene," Nature **438**, 197–200 (2005).
2. S. Chen, M. He, Y.-H. Zhang, V. Hsieh, Z. Fei, K. Watanabe, T. Taniguchi, D. H. Cobden, X. Xu, and C. R. Dean, "Electrically tunable correlated and topological states in twisted monolayer-bilayer graphene," Nature Physics **17**, 374–380 (2021).
3. M. Fan, J. Wu, J. Yuan, L. Deng, N. Zhong, L. He, J. Cui, Z. Wang, S. K. Behera, and C. Zhang, "Doping nanoscale graphene domains improves magnetism in hexagonal boron nitride," Advanced Materials **31**, 1805778 (2019).
4. Y. Zheng and T. Ando, "Hall conductivity of a two-dimensional graphite system," Phys. Rev. B **65**, 245420 (2002).
5. A. Shrestha, Y. Sumiya, K. Okazawa, T. Uwabe, and K. Yoshizawa, "Molecular understanding of adhesion of epoxy resin to graphene and graphene oxide surfaces in terms of orbital interactions," Langmuir **39**, 5514–5526 (2023).
6. A. Shrestha, Y. Sumiya, K. Okazawa, Y. Tsuji, and K. Yoshizawa, "Density functional theory study of adhesion mechanism between epoxy resins cured with 4,4'-diaminodiphenyl sulfone and 4,4'-diaminodiphenylmethane and carboxyl functionalized carbon fiber," Langmuir **40**, 21573–21586 (2024).
7. A. K. Geim and K. S. Novoselov, "The rise of graphene," Nature Mater **6**, 183–191 (2007).
8. S. G. Sharapov, V. P. Gusynin, and H. Beck, "Magnetic oscillations in planar systems with the dirac-like spectrum of quasiparticle excitations," Phys. Rev. B **69**, 075104 (2004).
9. Y. Gao, S. A. Yang, and Q. Niu, "Geometrical effects in orbital magnetic susceptibility," Phys. Rev. B **91**, 21440 (2015).
10. R. Kundu, "Tight-binding parameters for graphene," Modern Physics Letters B **25**, 163–173 (2011).
11. S. Reich, J. Maultzsch, C. Thomsen, and P. Ordejón, "Tight-binding description of graphene," Phys. Rev. B **66**, 035412 (2002).
12. R. Roldán, M. P. López-Sancho, and F. Guinea, "Effect of electron-electron interaction on the fermi surface topology of doped graphene," Phys. Rev. B **77**, 115410 (2008).
13. D. D. Koelling and G. O. Arbman, "Use of energy derivative of the radial solution in an augmented plane wave method: application to copper," Journal of Physics F: Metal Physics **5**, 2041–2054 (1975).
14. T. Takeda, "The scalar relativistic approximation," Zeitschrift für Physik B Condensed Matter **32**, 43–48 (1978).
15. M. Higuchi and A. Hasegawa, "Self-consistent relativistic linear augmented planewave method: Application to ybga2," Journal of the Physical Society of Japan **64**, 830–847 (1995).
16. M. Higuchi and A. Hasegawa, "Fermi surface of ceru2 within local-density functional theory," Journal of the Physical Society of Japan **65**, 1302–1311 (1996).
17. K. Higuchi, D. B. Hamal, and M. Higuchi, "Relativistic tight-binding approximation method for materials immersed in a uniform magnetic field: Application to crystalline silicon," Phys. Rev. B **91**, 075122 (2015).
18. D. B. Hamal, M. Higuchi, and K. Higuchi, "Calculation of magnetic oscillations via the magnetic-field containing relativistic tight-binding approximation method: Revisiting the de haas-van alphen effect," Phys. Rev. B **91**, 245101 (2015).
19. M. Gmitra, S. Konschuh, C. Ertler, C. Ambrosch-Draxl, and J. Fabian, "Band-structure topologies of graphene: Spin-orbit coupling effects from first principles," Phys. Rev. B **80**, 235431 (2009).
20. L. I. Schiff, *Quantum Mechanics* (McGRAW-HILL BOOK COMPANY, INC., 1955).
21. P. Hohenberg and W. Kohn, "Inhomogeneous electron gas," Phys. Rev. **136**, B864–B871 (1964).
22. W. Kohn and L. J. Sham, "Self-consistent equations including exchange and correlation effects," Phys. Rev. **140**, A1133–A1138 (1965).
23. M. Higuchi, D. B. Hamal, A. Shrestha, and K. Higuchi, "Reduced effective g-factor in graphene," Journal of the Physical Society of Japan **88**, 094707 (2019).
24. C. Kane and E. Mele, "Quantum spin hall effect in graphene," Phys. Rev. Lett. **95**, 226801 (2005).